JVI Accepted Manuscript Posted Online 20 September 2017
J. Virol. doi:10.1128/JVI.01352-17

Protective Humoral Immunity in the CNS Requires Peripheral CD19-Dependent Germinal Center Formation Following Coronavirus Encephalomyelitis

Jeffrey R. Atkinson[1,2], Cornelia C. Bergmann[1]#

[1]Department of Neurosciences, Lerner Research Institute, Cleveland Clinic Foundation, Cleveland, OH, USA

[2] School of Biomedical Sciences, Kent State University, Kent, OH, USA

Running Head: CD19-Dependent Humoral Immunity to CNS Viral Infection

#Address correspondence to Dr. Cornelia C. Bergmann, bergmac@ccf.org.

Word Count:

Abstract: 243

Importance: 149

Text: 6,549

Abstract

B cell subsets with phenotypes characteristic of naïve, non-isotype-switched, memory (B_{mem}), and antibody-secreting cells (ASC) accumulate in various models of central nervous system (CNS) inflammation, including viral encephalomyelitis. During neurotropic coronavirus JHMV infection infiltration of protective ASC occurs after T cell mediated viral control, and is preceded by accumulation of non-isotype switched IgD^+ and IgM^+ B cells. However, the contribution of peripheral activation events in cervical lymph nodes (CLN) in driving humoral immune responses in the infected CNS is poorly defined. CD19, a signaling component of the B cell receptor complex, is one of multiple regulators driving B cell differentiation and germinal center (GC) formation by lowering the threshold of antigen-driven activation. JHMV infected $CD19^{-/-}$ mice were thus used to determine how CD19 affects CNS recruitment of B cell subsets. Early polyclonal ASC expansion, GC formation, and virus-specific ASC were all significantly impaired in CLN of $CD19^{-/-}$ mice compared to wild type (wt) mice, consistent with lower and unsustained virus-specific serum Ab. ASC were also significantly reduced in the CNS resulting in increased infectious virus during persistence. Nevertheless, CD19 deficiency did not affect early CNS IgD^+ B cell accumulation. The results support that CD19 independent factors drive early B cell mobilization and recruitment to the infected CNS, while delayed accumulation of virus-specific, isotype switched ASC requires CD19 dependent GC formation in CLN. CD19 is thus essential for both sustained serum Ab as well as protective local Ab within the CNS following JHMV encephalomyelitis.

42 **Importance**

43 CD19 activation is known to promote GC formation and sustain serum Ab
44 responses following antigen immunization and viral infections. However, the
45 contribution of CD19 in the context of CNS infections has not been evaluated.
46 This study demonstrates that antiviral protective ASC in the CNS are dependent
47 on CD19 activation and peripheral GC formation, while accumulation of early-
48 recruited IgD^+ B cells is CD19-independent. This indicates that IgD^+ B cells
49 commonly found early in the CNS do not give rise to local ASC differentiation and
50 that only antigen-primed, peripheral GC-derived ASC infiltrate the CNS, thereby
51 limiting potentially harmful non-specific Ab secretion. Expanding our
52 understanding of activation signals driving CNS migration of distinct B cell
53 subsets during neuroinflammatory insults is critical for preventing and managing
54 acute encephalitic infections, as well as preempting reactivation of persistent
55 viruses during immune suppressive therapies targeting B cells in multiple
56 sclerosis (MS), such as Rituximab and Ocrelizumab.

Introduction

Infections of the central nervous system (CNS) commonly require a humoral immune component for effective long-term control (1-4). However, little is known about the signals driving B cell activation and differentiation during neurotropic infections or how peripheral factors affect local immunity in the CNS. Following CNS infection with a glial tropic sub-lethal variant of mouse hepatitis virus (MHV), designated JHMV-v2.2-1, both T and B cell priming occurs in draining cervical lymph nodes (CLN) (5-7). While virus specific CD4 and CD8 T cells are essential to clear infectious virus, virus specific ASC and sustained neutralizing IgG antibody (Ab) are required for long term control of persisting virus, which is only detectable by the ongoing presence of low levels of viral RNA (5, 8, 9). Virus-specific ASC in CLN are CD4-dependent (10) and reach peak frequencies at ~14 days post infection (p.i.) (7, 11), coincident with germinal center (GC) formation (12). However, their accumulation in the CNS is not robust until day 21 p.i., when more mature GC characterized by dark and light zones become evident (12). Irrespective of the temporal and spatial ASC organization in CLN, chemokine guidance mediated via CXCR3 ligands, predominantly CXCL10, is essential for protective ASC accumulation in the CNS (11, 13).

The extent to which peripheral mature GC formation imprints ASC migration to the CNS is still unclear despite the temporal correlation between GC formation and ASC accumulation in the CNS. Key lymphoid chemokines organizing B cell compartmentalization in follicles and GCs are CXCL12, CXCL13, as well as CCL19 and CCL21, which act through their cognate

receptors CXCR4, CXCR5, and CCR7, respectively (9, 14). Specifically CXCL13 contributes to GC formation by recruiting activated B and follicular helper $CD4^+$ T (T_{FH}) cells expressing CXCR5 (15-17). CXCL13 is also associated with lymphoid neogenesis in non-lymphoid tissue, such as joints during rheumatoid arthritis (18) and CNS meninges during some neuroinflammatory diseases, including multiple sclerosis (MS) and Lyme disease (19-23). However, despite impaired GC formation, $CXCL13^{-/-}$ mice infected with glia tropic JHMV mounted effective peripheral ASC and serum Ab responses (24). Importantly, the specific deficit in ASC and B_{mem} in the CNS did not affect virus control during persistence. Moreover, initial non-isotype-switched B cell recruitment into the CNS was not affected (24), similar to studies in Sindbis virus infection and experimental allergic encephalomyelitis (EAE) (25).

These results questioned the nature of activation signals required not only for effective ASC responses in the CNS, but also to mobilize early activated IgD^+ cells to the CNS, whose function and specificity is unknown. One critical signaling component promoting B cell receptor (BCR)-mediated activation and GC formation under conditions of low antigen (Ag) dose and/or limited pro-inflammatory stimuli is the BCR co-receptor CD19 (26). Together with CD21, also known as complement receptor type 2 (CR2), and CD81, CD19 forms a multimeric signal transduction complex on mature B cells (27-29). Activation and attachment of complement C3d, a cleavage product of complement C3, to Ag forms a covalent complex, which can lower the threshold for B cell activation by colligation of the BCR and coreceptor complex (28, 30, 31). The C3d-Ag complex

also acts directly on activated B cells in follicles and GC to enhance their survival (28, 32). Complement-mediated retention of Ag on follicular dendritic cells further promotes clonal selection of activated B cells in GCs. While many studies assessing the role of CD19 have focused on CD19$^{-/-}$ mice immunized with protein or inactivated virus, reports describing responses to replicating viruses are limited (26, 31). The latter revealed that CD19 is required for T cell-dependent responses such LCMV infection, but this requirement is overcome by infections associated with high viral dose exemplified by VSV (26). While a direct role of CD19 was not determined following peripheral HSV-1 infection, efficient humoral responses were dependent on complement C3 and CD21 (33). Overall both Ag and viral studies support a co-stimulatory role for CD19 in inducing long-term B cell memory, with CD19 playing a more prominent role in GC formation under limiting Ag conditions (26, 28, 31, 34).

The studies above focused largely on ASC and Ab responses to peripheral infections leaving the impact of CD19-dependent activation on B cell migration to inflamed tissue unclear. CNS inflammation is associated with accumulation of B cells in various differentiation and activation stages, independent of the insult, suggesting a common denominator in driving their initial activation (12, 35). Using the JHMV-induced encephalomyelitis model this study set out to identify a role of CD19 in driving early-activated B cells into the CNS as well as promoting antiviral ASC. Coincident with severely impaired GC formation, virus-specific ASC were significantly reduced in CLN and barely detectable in the CNS compared to wild type (wt) mice. While infected CD19$^{-/-}$

mice mounted virus-specific serum Ab, they were not sustained. Surprisingly, early polyclonal ASC expansion prior to GC formation was also significantly reduced. However, absence of BCR-CD19 co-ligation did not appear to affect early CNS B cell accumulation. The results further demonstrate that elevated persisting virus in the CNS, as a result of impaired humoral immunity, can still be effectively controlled by re-emerging T cell activity without causing increased clinical disease.

Methods

Mice, virus infection, and virus titer. C57BL/6 were purchased from the National Cancer Institute (Frederick, MD). B6.129P2(C)-*Cd19*$^{tm1(cre)Cgn}$/J mice (36) were purchased from The Jackson Laboratory (Bar Harbor, ME) and homozygous mice were utilized as CD19$^{-/-}$ mice. Female and male mice were housed at the Cleveland Clinic Lerner Research Institute under pathogen-free conditions. All animal procedures were executed in accordance with approved guidelines by the Cleveland Clinic Lerner Research Institute Institutional Animal Care and Use Committee. Mice of 6-7 weeks of age were infected by intracranial injection with 1,000 PFU of the gliatropic JHMV variant designated v2.2-1 (37). Infected animals were evaluated daily for clinical signs utilizing the following scale: 0, healthy; 1, hunched back and ruffled fur; 2, inability to correct to upright position or partial hind limb paralysis; 3, complete hind limb paralysis and wasting; 4, moribund or deceased. Virus titers within the CNS were determined in clarified supernatants via plaque assay with the murine delayed brain tumor (DBT) astrocytoma as previously described (37). Plaques were quantified following a 48 hour incubation at 37ºC.

Quantitative real-time polymerase chain reaction (PCR) gene expression analysis. Spinal cords and brains harvested from individual mice were snap-frozen, treated with 1 mL Trizol (Invitrogen, Grand Island, NY) and homogenized using a TissueLyser and stainless steel beads (Qiagen, Valenica, CA). RNA was extracted according to the manufacturer's instructions. DNA contamination was

eliminated via DNase I treatment for 30 minutes at 37ºC (DNA-free kit; Ambion, Austin, TX). cDNA was synthesized from RNA using Moloney murine leukemia virus (MMLV) reverse transcriptase (Invitrogen) and a 1:1 mixture of oligo (dT) primers and random primers (Promega, Madison, WI). Quantitative real-time PCR was performed using either SYBR Green Master Mix or Applied Biosystems Gene Expression Assays with Universal Taqman Master Mix on a 7500 Fast Real-Time PCR System (Applied Biosystems, Foster City, CA). Primers used for transcripts encoding glyceraldehyde 3-phosphate dehydrogenase (GAPDH), Tumor necrosis factor (TNF), a proliferation-inducing ligand (APRIL, TNFSF13), IL-21, CXCL9, CXCL10, viral nucleocapsid, and C3 (5'-AAGCATCAACACACCCAACA-3', 5'-CTTGAGCTCCATTCGTGACA-3') were used in conjunction with SYBR Green Master mix as described previously (8, 24, 38). GAPDH, activation-induced cytidine deaminase (AID), immunoglobulin gamma (IgG), gamma interferon (IFNγ), CXCR5, CCL19, CCL21, CXCL13, B-cell activating factor (BAFF, TNFSF13B), and IL-10 mRNA levels were determined using Taqman primers (Applied Biosystems). Transcript levels were calculated relative to the housekeeping gene GAPDH using the following formula: $2^{[CT(GAPDH) - CT(Target\ Gene)]} \times 1000$.

Mononuclear cell isolation and flow cytometric analysis

Cells were isolated from the CNS as described (24, 39). Briefly, brains harvested from PBS-perfused mice were mechanically homogenized in Dulbecco's PBS using ice-cold Tenbroeck grinders. The resulting suspension was centrifuged at

179 450 x g for 7 minutes at 4°C, supernatants stored at -80°C for subsequent
180 analysis, and cells resuspended in RPMI medium. Cells were adjusted to 30%
181 percoll (Pharmacia, Piscataway, NJ), underlayed with 1 ml 70% Percoll and
182 collected from the 30%/70% Percoll interface following centrifugation at 850 xg
183 for 30 minutes at 4°C. After washing cells were resuspended in fluorescence-
184 activated cell sorter (FACS) buffer and incubated with a mixture of mouse, goat,
185 and horse serum (1:1:1) and rat anti-mouse FcγIII/II mAb (2.4G2: BD Bioscience,
186 San Diego, CA) for 20 minutes on ice. Cells were then stained with specific
187 monoclonal Ab (mAb) to determine expression of cell surface markers for CD45
188 (30-F11), CD4 (L3T4), B220 (RA3-6B2), CD138 (281-2), CD95 (Jo2), CXCR4
189 (2B11), T-cell and B-cell activation antigen (GL7) (all from BD Pharmingen), CD8
190 (53-6.7), PD-1 (RMP1-30) (all from eBioscience), and CXCR3 (R&D Systems).
191 Cell surface expression of CXCR5 was determined via staining with biotin rat
192 anti-mouse CXCR5 mAb and streptavidin phycoerythrin (both from BD
193 Bioscience). Cells were then washed with FACS buffer, fixed with 2%
194 paraformaldehyde, and analyzed on a BD LSR II flow cytometer. Resulting data
195 was analyzed with FlowJo software (Tree Star Inc., Ashland, OR).
196
197 **Serum, brain supernatant, and neutralizing Ab quantification**
198 JHMV-specific IgG and IgM in serum and brain supernatant was quantified by
199 ELISA using plates coated with serum-free supernatant from infected DBT cells
200 and biotinylated goat anti-mouse IgG2a and IgM as detection Ab as described (7,
201 38). Ab titers are expressed as the log of the highest dilution with an optical

density value exceeding 3 standard deviations above the mean background. Titers for brain supernatants are expressed using the following formula: (absorbance at 450nm / 0.1) x dilution factor x total volume of clarified CNS supernatant. Neutralizing serum Ab was measured by incubation of serial 2-fold dilutions of heat inactivated serum from individual mice with 50 PFU JHMV in 96-well plates for 90 min at 37°C. DBT cells were added, and plates incubated at 37°C for 48 h. Neutralization titers represent the log of the highest average serum dilution that inhibited cytopathic effect.

ELISPOT

ASC were determined by ELISPOT as described previously (12, 24). Briefly, sterile, white 96-well filter plates with 0.45 µm pore size hydrophobic PVDF membrane (Merck Millipore, Billerica, MA) were stripped with 70% ethanol for 2 minutes, washed with 0.1M sodium bicarbonate buffer, and coated with either polyclonal goat anti-mouse Ig (Life Technologies, Eugene, OR) at a concentration of 2 mg/ml or undiluted virus supernatant for approximately 16 hours at 4°C. Wells were washed with washing buffer (0.05% Tween20 in 1xPBS) and blocked with 5% FCS in RPMI medium for 2 hours at 37°C. Blocking buffer was replaced with cell suspensions at serial dilutions in triplicate in RPMI medium. Plates were incubated at 37°C for 4 hours, then washed thoroughly to remove cells. After addition of biotinylated rabbit anti-mouse IgG (Southern Biotech, Birmingham, AL) at a concentration of 0.5 µg/mL, plates were incubated for ~16 hours at 4°C, subsequently washed with washing buffer, and

incubated with streptavidin horseradish peroxidase for 1 hour at 25°C. Following washes with washing buffer and 1xPBS, respectively, diaminobezadine (DAB) solution was added to visualize spots. Once spots had developed sufficiently, the reaction was stopped by flushing wells with H_20 and plates left to dry in the dark. Plates were scanned and spots quantified via Immunospot (Cellular Technologies Ltd., Shaker Heights, OH). Threshold criteria for spot size was defined as between 0.0009 and .2257 mm^2.

Immunohistochemistry

CLN from PBS-perfused mice were snap-frozen in Tissue-Tek OCT compound (Sakura Finetex, Torrance, CA) and sectioned at 10 µm using a Thermo Shandon cryostat. Slide-mounted tissue sections were fixed with ice cold 70% acetone for 5 min, blocked with 5% bovine serum albumin and 10% goat serum for 1 h, and stained with rat anti-mouse B220 mAb (BD biosciences), and rabbit anti-mouse CD3 polyclonal Ab (Abcam, Cambridge, MA), and rat anti-mouse FITC conjugated GL7 mAb (BD Biosciences) overnight at 4°C. Sections were then incubated with secondary Ab using Alexa Fluor 594 goat anti-rat (Life Technologies, Grand Island, NY) and Cy5 goat anti-rabbit (Life Technologies, Grand Island, NY) Ab for 1 h at room temperature. Sections were mounted with Vectashield Hard Set Mounting Medium with DAPI (40,6-diamidino-2-phenylindole) (Vector Laboratories, Burlingame, CA) and examined using a Leica TCS SP5 II confocal microscope (Leica Microsystems, Exton, PA).

248 **Statistical analysis**

249 All results are expressed as the mean ± standard error of the mean (SEM). Data
250 were plotted and statistical significance determined utilizing GraphPad Prism 6
251 software. Statistically significant differences are denoted by *$p < 0.05$, **$p < 0.01$,
252 ***$p < 0.001$, unless otherwise noted.

Results

CD19 deficiency abrogates peripheral GC formation following CNS infection

CLN are the predominant site of both T cell and ASC expansion following JHMV infection, consistent with CLN as the draining site for CNS-derived Ag (5, 40-42). Temporal analysis of GC formation in CLN following JHMV infection using GL7 to identify GC B cells previously showed formation of $GL7^+$ foci as early as day 7 p.i., more defined structures by day 14 p.i., and segregation into light and dark zones by day 21 p.i. (12). To assess whether accumulation of ASC within the CNS is dependent on CD19 signaling and GC formation in the periphery, JHMV infected $CD19^{-/-}$ and wt mice were initially compared for GC formation in CLN. In wt CLN, defined structures of $GL7^+$ $B220^+$ B cells started to form at day 14 p.i. and were robust by day 21 p.i. (Fig. 1A), confirming previous results (12). By contrast, in the absence of CD19, $GL7^+$ cells were very sparse and scattered at day 14 p.i. Although GC were evident in some follicles by day 21.p.i., they were small in size and disorganized compared to those in wt mice (Fig. 1A). $GL7^+$ B cells were scattered within the follicle (white arrows) without forming structures resembling GC architecture. Quantitative evaluation of $GL7^+$ area by immunofluorescence highlights significantly reduced reactivity in $CD19^{-/-}$ compared to wt mice, especially at day 21 p.i. , when pixels per frame were 18-fold reduced (Fig. 1B). Impaired GC formation could not be attributed to disrupted lymphoid organization as B cell follicle formation and lymphoid architecture is intact in naïve $CD19^{-/-}$ mice (43).

The extent of impaired GC formation was further confirmed by flow cytometry using the B220^{+} GL7^{+} CD95^{+} phenotype to identify GC B cells (Fig. 1C). The population of GL7^{+} CD95^{+} B cells in CLN of both naive wt and CD19$^{-/-}$ mice was below 0.5%, consistent with no or sparse GC activity. In wt mice GL7^{+} CD95^{+} B cells started to emerge at day 5 and continued to increase to ~3% by day 14.p.i., consistent with anatomical GC formation. The frequency of GC phenotype B cells was maintained at ~3-4% throughout days 21 and 28 p.i. In contrast, GL7^{+} CD95^{+} B cells were only slightly elevated to <1% in CD19$^{-/-}$ mice and remained barely detectable throughout infection (Fig. 1C). Functionally, GC B cells are characterized by upregulation of activation-induced cytidine deaminase (AICDA), an enzyme required for somatic hypermutation and class switch recombination to increase Ab diversity and affinity. As B cell maturation can occur in the absence of GC (24, 25, 44), we also assessed transcript levels of the gene encoding AICDA (*aicda*). In CLN of infected wt mice, the progressive increase of *aicda* mRNA levels from day 7 to 21 p.i. correlated with GC formation and maturation (Fig. 1D). While CD19$^{-/-}$ mice exhibited modestly increased *aicda* mRNA levels in CLN between days 7 and 21 p.i., these levels did not significantly differ from naïve CD19$^{-/-}$ mice until day 21 p.i. (Fig. 1D). These results demonstrate a retarded and diminished capacity to initiate GC reactions in JHMV-infected CD19$^{-/-}$ relative to wt mice. Nevertheless, the relative population of GL7^{+} CD95^{+} B cells in CD19$^{-/-}$ CLN only reached ~15% of wt levels at day 21 p.i., while *aicda* mRNA levels reached ~40% of wt levels, suggesting that CD19$^{-/-}$

B-cells exhibit modest maturation capacity despite severely impaired GC formation.

To support the notion that deficient GC formation is a result of poor B cell activation in the absence of CD19 rather than extrinsic factors related to GC formation, we assessed transcript levels for several chemokines and cytokines regulating B cell migration and differentiation (Fig. 2). Compared to infected wt mice, CD19$^{-/-}$ mice exhibited no significant changes in relative levels or kinetics of mRNAs encoding CXCL13, CCL19 or CCL21, lymphoid chemokines regulating B cell migration within follicles (14) (Fig. 2). The CXCL13 chemokine receptor CXCR5 is up-regulated on B cells migrating to and forming GC (15, 45). It is also highly expressed by follicular helper T cells (T_{FH}), which are essential for GC formation, maintenance, B cell differentiation and survival by producing IL-21. Although *cxcr5* transcripts were elevated in CLN of CD19$^{-/-}$ mice throughout infection, differences only reached statistical significance at day 21 p.i. (Fig. 2). *Il21* mRNA levels were not significantly altered in the absence of CD19 (Fig. 2), consistent with similar T_{FH} cell frequencies characterized by their PD-1^{+}CXCR5^{+} phenotype using flow cytometry in both wt and CD19$^{-/-}$ mice (data not shown). Furthermore, transcript levels of the *Tnfsf13b* gene, which encodes the survival factor B-cell activation factor (BAFF), were also similar between both groups suggesting no deficits in retaining B cell viability. We also assessed upregulation of transcripts encoding complement protein C3. C3-Ag adducts not only lower the threshold for B cell activation by co-ligation of the CD21/CD19/CD81 BCR co-receptor, but also enhance B cell survival in follicles and GC (32). CNS infection

321 indeed resulted in significant upregulation of *c3* mRNA in both groups at day 7 to
322 14 p.i. and remained elevated to day 21 p.i. Overall these results suggested that
323 the absence of CD19 did not impair cues for B cell localization to and trafficking
324 between anatomical structures of the CLN. The deficit in GC formation more
325 likely resides in deficient CD19 engagement either directly or indirectly via the
326 complement C3d binding receptor CD21 (27, 32).

327 **Impaired GC formation is associated with induction of, but reduced and**
328 **rapid decline in, virus-specific humoral responses in the periphery**

329 Impaired GC formation in CLN was also a hallmark of CXCL13$^{-/-}$ mice
330 infected with JHMV. However, differentiation of B cells into virus specific IgG
331 ASC was only reduced by ~25% in the CLN and 50% in in the CNS (24).
332 Modestly impaired, but not abrogated, virus-specific serum Ab in the absence of
333 CXCL13 confirmed that formation of mature GC in CLN is not an absolute
334 requirement for development of peripheral or CNS humoral immunity. We
335 therefore assessed how severely impaired GC formation in CD19$^{-/-}$ affects JHMV-
336 specific serum Ab throughout infection. Virus-specific IgM levels were below
337 detection at day 7 p.i. in CD19$^{-/-}$ mice, but reached similar levels to wt mice by
338 day 14 p.i. (Fig. 3A). However, while wt mice sustained virus-specific IgM levels
339 out to day 28 p.i., they were progressively lost after day 14 p.i. in CD19$^{-/-}$ mice.
340 Virus-specific IgG2a was induced in both mouse groups by day 7 p.i. and
341 increased by day 14 p.i. (Fig. 3A). However, the levels were lower in the absence
342 of CD19 reaching ~3 $\log_{10}$ relative to ~4-4.5 $\log_{10}$ in wt mice. Furthermore, while
343 virus-specific serum IgG2a increased slightly in wt mice by day 21 p.i. and then

stabilized, it already started to decline by day 28 p.i. in CD19$^{-/-}$ mice. Importantly, although neutralizing serum Ab was initially reduced in infected CD19$^{-/-}$ relative to wt mice at day 7 p.i, it reached levels found in wt mice by day 14 p.i. However, distinct from the gradual increase of neutralizing Ab throughout infection in wt mice, it significantly declined by day 28 p.i. in CD19$^{-/-}$ mice (Fig. 3A). Thus, despite impaired GC formation in the absence of CD19, virus-specific serum Ab responses were induced, albeit with delayed kinetics, at lower levels, and shorter longevity. The inability of serum Ab to be maintained supported a critical role for CD19 in generation of both IgM and isotype switched long-lived ASC (31).

Induction, but not maintenance of virus-specific serum Ab prompted us to investigate the kinetics of virus-specific IgG ASC accumulation in CLN and bone marrow (BM) by ELISPOT analysis (Fig. 3B, C). Virus specific IgG ASC emerged at day 7 in CLN of wt mice, reached peak frequencies at day 14 p.i., and declined by day 21 p.i., consistent with previous data (7, 11, 46). Although virus-specific IgG ASC followed similar kinetics in CD19$^{-/-}$ mice, peak frequencies were reduced by ~70% compared to wt mice and dropped to barely detectable levels by day 21 p.i. Furthermore, contrasting the modest increase in virus-specific ASC in BM by day 21 p.i., virus-specific IgG ASC remained at baseline levels in BM of CD19$^{-/-}$ mice (Fig. 3C). Impaired ASC maturation was supported by assessment of spot size as an indicator for ASC Ab secretion rate (Fig. 3B, C). On average, ASC derived from WT CLN and BM at day 14 and 21 p.i., respectively, formed more intense spots with an increased diameter compared to CD19$^{-/-}$ counterparts, suggesting higher rates of IgG secretion. Sparse GC formation

following JHMV infection of CD19$^{-/-}$ mice thus coincides with reduced virus-specific ASC maturation and longevity. These results indicated CD19 is essential to drive activation and differentiation of high affinity virus-specific ASC competent to egress CLN and migrate to survival niches in BM (47).

CD19 deficiency severely diminishes peripheral ASC expansion following CNS infection

Impaired virus-specific ASC and serum responses as early as day 7 p.i. were consistent with a defect in early activation potentially due to the absence of complement mediated costimulation through CD21. Moreover, the peak of virus-specific ASC at day 14 p.i. in CLN following JHMV infection is preceded by a peak in polyclonal ASC expansion at day 7 p.i. (11, 12). To assess whether CD19 deficiency specifically affected virus-specific ASC, overall ASC expansion in CLN was monitored by flow cytometry using CD138 as a phenotypic marker (Fig. 4A, B). The frequency of CD138^{+} B cells was reduced by ~70 % relative to wt mice at day 7 p.i. prior to expansion of virus specific ASC and remained low throughout days 14 to 28 p.i. (Fig. 4). Similar numbers of B220^{+} B cells in CLN of both groups during infection indicated no overall deficiencies in the B cell compartment or recruitment to CLN following infection (data not shown). These data were consistent with a polyclonal defect in early B cell activation in CD19$^{-/-}$ mice following JHMV infection preceding impaired generation of virus specific ASC. Taken together, these results demonstrate a diminished capacity to initiate GC reactions resulting in impaired differentiation of long-lived ASC in the absence of CD19 in the periphery.

CD19 deficiency severely diminishes CNS humoral responses

ASC expanding prior to GC formation in CLN appear not to have egress or migration capacity, as ASC do not emerge in the CNS until 14 days p.i. and only prominently increase thereafter (7, 11, 24, 46). This observation suggests accumulation of ASC in the CNS is dependent on differentiation in GCs. Moreover, unlike CXCR4 driven migration of ASC to BM, ASC accumulation in the CNS is dependent on CXCR3 expression (11). We therefore assessed whether the few ASC primed in CLN of CD19$^{-/-}$ mice nevertheless traffic to the infected CNS, as observed in CXCL13$^{-/-}$ mice (21). Measurement of virus-specific IgG ASC by ELISPOT revealed similar frequencies at day 14 p.i. when comparing brain or spinal cords of wt and CD19$^{-/-}$ mice, respectively (Fig. 5A). However, while frequencies in wt mice increased by day 21 p.i. and remained steady at day 28 p.i., they never increased in the CNS of CD19$^{-/-}$ mice. Overall, virus-specific ASC frequencies were significantly higher in spinal cords than brains in wt mice at day 21 and 28 p.i., consistent with their preferential accumulation at the site of persistence and elevated inflammation (48). The differences between ASC frequencies were therefore especially pronounced in spinal cords, amounting to an almost 10-fold disparity, whereas differences were only 3-4 fold in the brain (Fig. 5A). Similar to CLN, average spot sizes of virus-specific CD19$^{-/-}$ ASC were also reduced at days 21 and 28 p.i. compared to wt ASC, reflecting poor affinity maturation and differentiation. The paucity in virus-specific ASC in the brain was supported by direct analysis of supernatants from brain homogenates for virus-specific IgG2a Ab, the most abundant and protective

413 Ab isotype during JHMV infection (7, 49, 50). Compared to the progressive
414 increase of virus-specific IgG2a from day 14 to 28 p.i. in wt mice, the levels were
415 barely above background in CD19$^{-/-}$ mice (Fig. 5B).

416 To ascertain that CD19 deficiency affected overall ASC CNS migration
417 independent of specificity we monitored accumulation of ASC via expression of
418 mRNA encoding IgG and IgM heavy chains, which are expressed highly in ASC
419 compared to non Ab secreting B cells (8). Both brains and spinal cords of
420 infected wt mice exhibited a significant increase in IgG heavy chain mRNA by 14
421 days p.i., which was further elevated at days 21 through 28 p.i. (Fig 6A). As
422 anticipated CD19$^{-/-}$ mice exhibited significantly decreased transcript levels
423 throughout days 14 p.i. to 28 p.i. (Fig. 6A). Although a slight trend towards
424 elevated transcript levels was noted in spinal cords, the levels at day 28 p.i. did
425 not even reach those of wt mice at day 14 p.i. To delineate potential factors
426 abrogating accumulation of ASCs within the CNS of CD19$^{-/-}$ mice, we used flow
427 cytometry to assess CXCR3 expression on CD138^{+} ASCs in the CLN (Fig. 6B).
428 CXCR3 is upregulated by IFNγ and essential in driving ASC migration to and
429 entry into the CNS parenchyma (11). CD19$^{-/-}$ mice expressed significantly
430 reduced frequencies of CXCR3^{+} ASCs in the CLN throughout infection, with
431 differences most prominent at day 14 p.i. (Fig. 6B). However, the mean
432 fluorescent intensity (MFI) of CXCR3^{+} was similar between wt and CD19$^{-/-}$ ASCs
433 (Fig. 6C). These data suggest that there is no inherent deficit in the ability of
434 CD19$^{-/-}$ ASCs to express CXCR3. Similarly to CXCR3, CXCR4 is upregulated
435 during ASC differentiation (11, 51). Interactions with its ligand, CXCL12, are

important in mediating ASC homing to, and retention within, the BM (47, 51). CD19$^{-/-}$ mice also demonstrated a significant reduction in the frequency of ASCs expressing CXCR4 in the CLN, beginning at day 14 p.i. and continuing throughout infection (data not shown). As was the case with CXCR3, the MFI of CXCR4 on ASCs did not differ between wt and CD19$^{-/-}$ mice (data not shown).

We further assessed how CD19 deficiency affects overall B cell recruitment using CD45^{hi} and B220 as expression markers of infiltrating B cells. There were no differences in total CNS cell yields or frequencies of CD45^{hi} infiltrating bone marrow derived cells. CD8^{+} and CD4^{+} T cells were also similar between the groups (data not shown), confirming no overall deficits in leukocyte trafficking to the CNS. Although a ~40% reduction in the frequency of B220^{+} B cells in the CNS was noted at 7 days p.i., frequencies were similar to wt mice by days 14 and 21 (Fig. 7). Moreover, ~60% of B220^{+} B cells expressed IgD^{+} in both groups at days 7 and 14 p.i., indicating that a majority of these B cells are undifferentiated. By day 21 p.i., the proportions decreased similarly to ~25%. These results suggest that CD19 has a minor impact on migration of IgD^{+} early-activated B cells into the CNS following JHMV infection, but specifically affects overall ASC accumulation at day 14 p.i. and thereafter.

The deficit in CNS humoral immunity is associated with increased infectious virus balanced by reactivation of T cell responses

The severe deficit in virus-specific ASC and antiviral IgG2a in the CNS of JHMV-infected mice predicted loss of virus control during the persistent phase of infection, which requires local ASC (7, 49, 50, 52). Infectious virus load was

similar and even lower in the CNS of CD19$^{-/-}$ compared to wt mice at day 7 and 14 p.i. (Fig. 8A), consistent with T cell-mediated control. However, whereas wt mice reduced infectious virus to below detection by day 21 p.i., it remained detectable between day 14 and 28 p.i. in the absence of CD19 (Fig. 8A). The inability to maintain effective virus control was confirmed by elevated, and even increasing, transcript levels of viral RNA encoding nucleocapsid protein in both brain and spinal cord comparing day 21 and 28 p.i. (Fig. 8B), although the increase was modest. Importantly however, mice also did not show signs of increased clinical disease (data not shown), distinct from mice totally deficient in virus specific Ab production, in which vastly increasing virus is associated with worsening clinical disease (52-54). Although T cells did not increase in the CNS during persistence in CD19$^{-/-}$ mice (data not shown), we assessed reemergence of T cell effector activity to explain partial ongoing viral control during persistence. IFNγ is the most critical cytokine essential for JHMV control (5, 55, 56). IFNγ transcripts peaked to similar levels at day 7 p.i. in both the brain and spinal cord of CD19$^{-/-}$ and wt mice, confirming effective T cell stimulation by virus Ag presentation (Fig. 8C). IFNγ mRNA levels dropped by days 10 and 14 p.i. coincident with viral control and were similarly low in both groups at day 21 p.i., implying minimal *in vivo* stimulation and antiviral T cell activity. However, by day 28 p.i. IFNγ mRNA levels were significantly elevated in both brains and spinal cords of CD19$^{-/-}$ mice. These results indicated that elevated persisting viral load triggers retained or reemerging T cells to produce IFNγ and exert antiviral activity.

To provide evidence for reemergence of other T cell functions as well as IFNγ-dependent activities, both brains and spinal cords were temporally screened for expression of factors associated with increased T cell function (Fig. 9). IL-21 not only enhances B cell differentiation in CLN, but also enhances and prolongs CD8 T cell function within the CNS (10). While IL-21 was similarly regulated in the CNS of wt and CD19$^{-/-}$ mice out to day 14 p.i., it was sustained and even increased in both brain and spinal cord of CD19$^{-/-}$ compared to wt mice during persistence, reaching statistically significant differences by day 28 p.i. Surprisingly, transcript levels of the lymphoid chemokine CXCL13, which regulates migration of IL-21 expressing CXCR5^{+} T cells was also notably elevated at day 28 p.i. in the CNS of CD19$^{-/-}$ mice. Increased functional IFNγ activity in the CNS of CD19$^{-/-}$ mice *in vivo* was supported by elevated IFNγ inducible *Tnfsf13b* and *cxcl9* mRNA relative to wt mice, specifically at day 28 p.i. By contrast, *C3* mRNA as an activation marker peaked in the brain at day 7, and was only marginally increased at day 28 p.i. in the absence of CD19. Surprisingly, spinal cords revealed increasing *C3* mRNA levels throughout persistence on both groups. Lastly, *IL-10* mRNA, expressed most prominently by CD4 T cells during JHMV infection (57), peaked in both groups and organs at day 7 p.i.,and declined during persistence, but was sustained at higher levels in CD19$^{-/-}$ mice, indicative of elevated regulatory T cell activity (58, 59). Assessment of the CCR7 binding lymphoid chemokines CCL19 and CCL21, known to be expressed in the inflamed CNS (60), revealed surprisingly distinct patterns between wt and CD19$^{-/-}$ mice. Compared to wt mice, CCL19 mRNA was

505 consistently elevated in brains of CD19$^{-/-}$ mice throughout infection, whereas it
506 was mainly increased at day 28 in spinal cords. Unexpectedly, *CCL21* mRNA
507 levels were vastly increased at basal levels in the CNS of CD19$^{-/-}$ mice, but
508 remained unaltered by infection, similar to naïve wt mice. Overall the data imply
509 that re-triggering of T cell activity by elevated virus replication in settings of
510 impaired humoral immunity potentially contributes to steady-state viral control
511 during JHMV persistence.

512 **Discussion**

513 A variety of human viral CNS infections, including those caused by
514 measles, mumps, rubella, polio, varicella zoster, herpes simplex and Japanese
515 encephalitis virus (JEV), are characterized by intrathecal Ab in the cerebral spinal
516 fluid (CSF), consistent with local ASC (2, 61-64). Overall Ab detection is more
517 transient in cases of acute encephalitis, but persists during chronic disease such
518 as measles virus-associated subacute sclerosing panencephalitis (65, 66).
519 Although the role of intrathecal humoral responses in humans is difficult to
520 assess, they correlate with protective functions during JEV encephalitis (67),
521 CNS retrovirus infection (68-70) and HTLV-I-associated myelopathy
522 (70). Experimental CNS infections in rodents support an essential local
523 protective role of ASC, as evidenced by infections established by Sindbis, rabies,
524 and neurotropic coronaviruses (3, 11, 54, 71-75). Sustained Ab output by local
525 ASC provides a potent non-lytic mechanism of immune control potentially
526 beneficial for a variety of neurotropic infections prone to persist. However, little is
527 known about peripheral activation signals and the necessity of GC formation in
528 regulating B cell migration and accumulation to the CNS.

529 Expression of the lymphoid chemokines CXCL13 and CCL19/21 within the
530 CNS has been associated with formation of ectopic follicle-like structures
531 harboring multiple B cell differentiation phenotypes giving rise to *de novo* local Ab
532 production (76-78). Upregulation of B cell survival factors (8, 79, 80) is thought to
533 contribute to clonal B cell expansion and local humoral responses distinct from
534 those occurring systemically. However, follicle-like structures have not been

535 observed in experimental viral encephalomyelitis (12, 81) suggesting activation
536 and GC formation in draining lymphoid organs imprints activated B cells for
537 migration to the inflamed site. As CD19 is a key signaling component initiating B
538 cell activation as well as driving GC formation, we assessed the relevance of
539 CD19 in humoral responses to neurotropic JHMV infection. As anticipated,
540 based on sparse peripheral replication and consequently Ag load (82), GC
541 formation was significantly impaired in the absence of CD19. Despite induction of
542 virus-specific serum IgG and neutralizing Ab, both IgM and IgG responses were
543 overall reduced and not sustained. Reduced anti-virus serum Ab, lower virus-
544 specific ASC and very scant accumulation of IgG ASC in BM are consistent with
545 lesser differentiation and longevity of isotype-switched CD19$^{-/-}$ ASC compared to
546 wt ASC.

547 Contrasting scant migration to BM, virus-specific ASC trafficking to the
548 CNS was initially similar to wt mice. However, their ongoing accumulation was
549 significantly impaired after day 14 p.i. The more prominent defect in spinal cord
550 reflects the overall enhanced ASC accumulation in spinal cord relative to brain
551 associated with increased and sustained expression of ASC promoting factors
552 (Fig. 9), as shown previously in wt mice (48). Initial recruitment of virus-specific
553 ASC to the CNS, but not BM, supports the notion that CXCR3 driven recruitment
554 to the inflamed site overrides CXCR4 driven recruitment to BM (46). Similar
555 CXCR3 expression levels on CD19$^{-/-}$ vs wt ASC in CLN, irrespective of their low
556 numbers, implies that defective progressive accumulation of ASC is due to their
557 less differentiated, short-lived phenotype as a result of impaired GC formation,

558 rather than an inherent defect in migration or ASC promoting factors in the CNS
559 of CD19$^{-/-}$ mice.

560 JHMV infection of CXCL13$^{-/-}$ mice also revealed impaired GC formation
561 with reduced frequencies of GL7^{+} B cells (24). Nevertheless, distinct from CD19$^{-/-}$
562 mice, virus-specific serum Ab responses were not significantly impaired
563 throughout day 21 p.i., consistent with similar ASC in BM and only slightly
564 reduced ASC in CLN. Although ASC in the CNS were reduced by 50% in
565 CXCL13$^{-/-}$ mice they were sufficient to control persisting viral RNA. Potential
566 differences may reside in lymphoid structure. While CXCL13$^{-/-}$ mice are devoid of
567 most lymph nodes, they retain cervical lymph nodes (45). However, the absence
568 of B cell follicles and disrupted lymphoid architecture likely alters typical migration
569 patterns. By contrast, CD19$^{-/-}$ mice exhibit normal lymphoid architecture with
570 intact B cell follicles (34), which may put more restraints on CD4 T cell-B cell
571 interactions. Irrespectively, the absence of CD19 leads to more severely impaired
572 generation of protective ASC during JHMV infection compared to CXCL13$^{-/-}$
573 mice. An early defect in B cell activation was already noted by reduced overall
574 expansion of ASC, prior to detection of virus-specific ASC. While the early
575 increase in ASC was previously attributed to IFNα/β-induced bystander activation
576 similar to influenza virus and WNV (83, 84), our results implicate a role for CD19
577 co-receptor activation via CD21 co-ligation by virus/C3d adducts. JHMV infection
578 resulted in a robust increase of *C3* mRNA in both CLN and the CNS. Viral
579 Ag/C3d mediated activation of the BCR co-receptor can thus reduce the
580 threshold for B cell activation in the periphery as well as the CNS, where

581 astrocytes, microglia, and potentially neurons and oligodendrocytes are likely
582 sources of C3 (85-87). Surprisingly however, early-activated IgD^+ B cells
583 recruited to the CNS were not altered by CD19 deficiency, suggesting BCR
584 independent signals drive their trafficking to the CNS. *In vitro* stimulation to
585 assess virus specificity in this population provided no evidence for these early B
586 cells as precursors of ASC (88). The nature of signals driving IgD^+ B cells to the
587 CNS during infection, as well as their role, thus remains to be determined, but
588 likely involves TLR driven signals (89, 90).

589 The biological impact of significantly impaired ASC within the CNS was
590 manifested by the inability of $CD19^{-/-}$ mice to control infectious virus during
591 persistence. Surprisingly, elevated viral load triggered T cell re-activation as
592 evidenced by reemerging IFNγ mRNA in both brains and spinal cords. Biological
593 IFNγ function was directly reflected by coincidently increased expression of IFNγ
594 inducible CXCL9 and CXCL10 mRNA (8). Although retention of both CD4 and
595 CD8 T cells in the CNS during persistence make them likely sources of IFNγ, *de*
596 *novo* recruitment of T cells cannot be excluded. In this context it is interesting to
597 note that *IL-21* mRNA levels were also increased, suggesting IL-21 contributes to
598 reinvigorating local CD8 T cell effector function (10). Together these data
599 suggest that persisting viral replication in the absence of protective ASC is kept
600 in check by reemerging T cell activity. The significantly higher constitutive levels
601 of the CCR7 binding chemokine CCL21 in both the brain and spinal cord, but not
602 CLN, of $CD19^{-/-}$ mice is also of interest. Elevated CCL21 mRNA was also noted
603 in $CXCL13^{-/-}$ and $CXCR3^{-/-}$ mice (11, 24). Following infection with the JHMV

604 heterologous MHV-A59 strain, CCR7 ligands produced by CNS stromal cells
605 were crucial to support recruitment and local re-activation of antiviral CD8+ T
606 cells (91). The latter studies indicated that CNS stromal cells generate confined
607 microenvironments that control T cell immunity and protect the host from lethal
608 neuroinflammatory disease. Surprisingly CD19$^{-/-}$ mice did not exhibit increased
609 clinical symptoms or disability at day 28.p.i., suggesting CNS pathology
610 manifested in demyelination and axonal damage was not significantly worsened.
611 Possible explanations reside in CCR7-mediated restraint of T cell function to
612 perivascular spaces and or elevated protective IL-10. In summary, the effect of
613 CD19 deficiency on JHMV-induced humoral responses was overall similar to
614 reduced GC formation in peripheral infection models associated with limited viral
615 antigen (26, 31). Moreover, the results are the first to demonstrate that protective
616 ASC in the CNS are dependent on CD19 activation. By contrast, CD19-
617 independent accumulation of early recruited IgD^{+} B cells to the CNS suggests
618 independent activation mechanisms drive the emergence of early versus more
619 differentiated, isotype-switched B cells accumulating in the CNS as GCs are
620 formed in the periphery. A better understanding of distinct B cell subsets in the
621 CNS is essential to preempt reactivation of persistent viruses in the CNS during
622 immune suppressive therapies (92, 93) as well as combat disease susceptibility
623 to acute encephalitic arboviral infections.

Acknowledgements

This work was supported by US National Institutes of Health grant NS086299. The funding source had no involvement in the study design, writing of the manuscript, decision to submit, or collection, analysis, and interpretation of data. We sincerely thank Dr. Mi-Hyun Hwang for viral CNS infection.

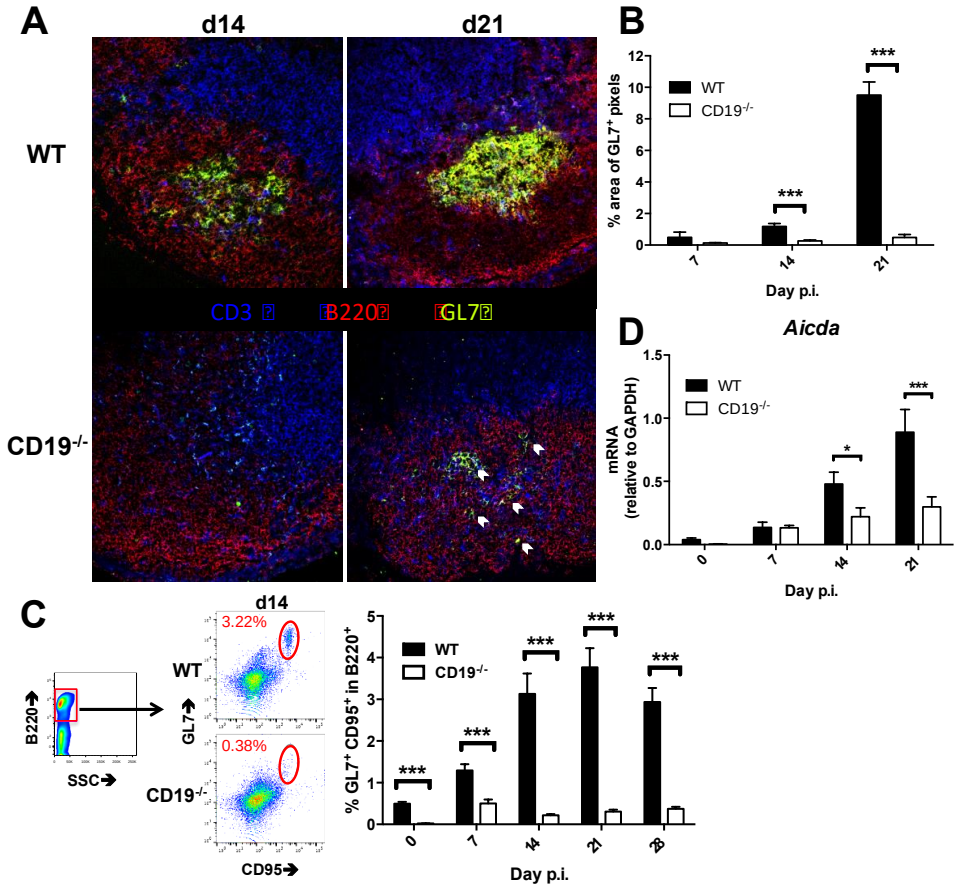

Figure 1. Infected CD19$^{-/-}$ mice exhibit diminished GC in CLN. WT and CD19$^{-/-}$ mice were infected with sublethal JHMV and CLN harvested at indicated times for histology, flow cytometric analysis and gene expression. A) Representative images of fluorescent immunohistochemistry performed at days 14 and 21 p.i.. Sections were stained for T cells (CD3, blue), B cells (B220, red), and activated GC B cells (GL7, green). Images were taken at 40x magnification. B) Percentage of pixels per image frame resulting from GL7^{+} staining in CLN follicles. Bars represent the mean percentage ± SEM of GL7^{+} pixels per frame from 2-3 frames per mouse from 2-6 mice per time point. C) Flow cytometry of CLN suspensions stained for B220, GL7, and CD95, and gated as indicated. The bar graph shows percentages of GL7^{+} CD95^{+} cells within total B cells over time. Data represent the mean ± SEM of 2-4 individual mice per time point per group from 4 separate experiments. D) CLN tissue was assessed for *Aicda* RNA transcript levels by rt-PCR over time. Data represent the mean ± SEM transcript levels relative to *gapdh* mRNA of individual mice from 2 separate experiments, each comprising 3-

645 5 individual mice per time point and group. Statistically significant differences
646 between wt and $CD19^{-/-}$ mice denoted by *$p < 0.05$, ***$p < 0.001$.

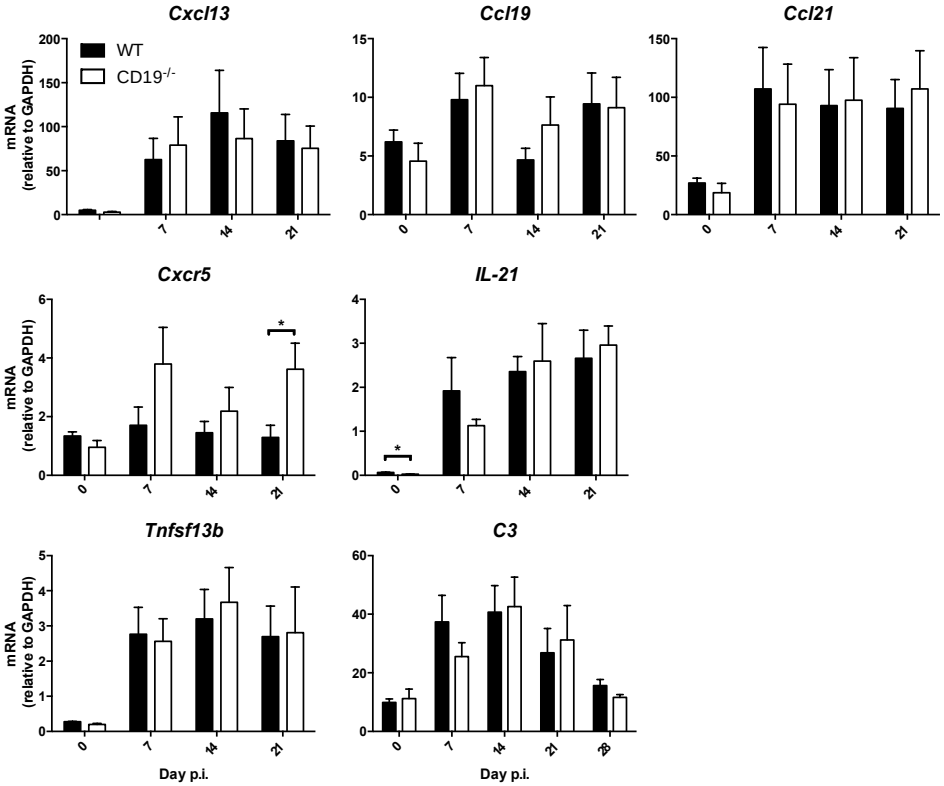

Figure 2. CD19 deficiency does not impair expression of factors promoting GC formation within CLN. CLN harvested from infected wt and CD19$^{-/-}$ mice at the indicated times p.i. were analyzed for mRNA expression levels of Cxcl13, Ccl19, Ccl21, Cxcr5, Il-21, Tnfsf13b (BAFF), and complement C3. Data represent the mean ± SEM transcript levels relative to *gapdh* mRNA of individual mice from 2 separate experiments, each comprising 3-5 individual mice per time point and group. Statistically significant differences between wt and CD19$^{-/-}$ mice, determined by unpaired *t* test, are denoted by *$p < 0.05$, ** $p < 0.01$.

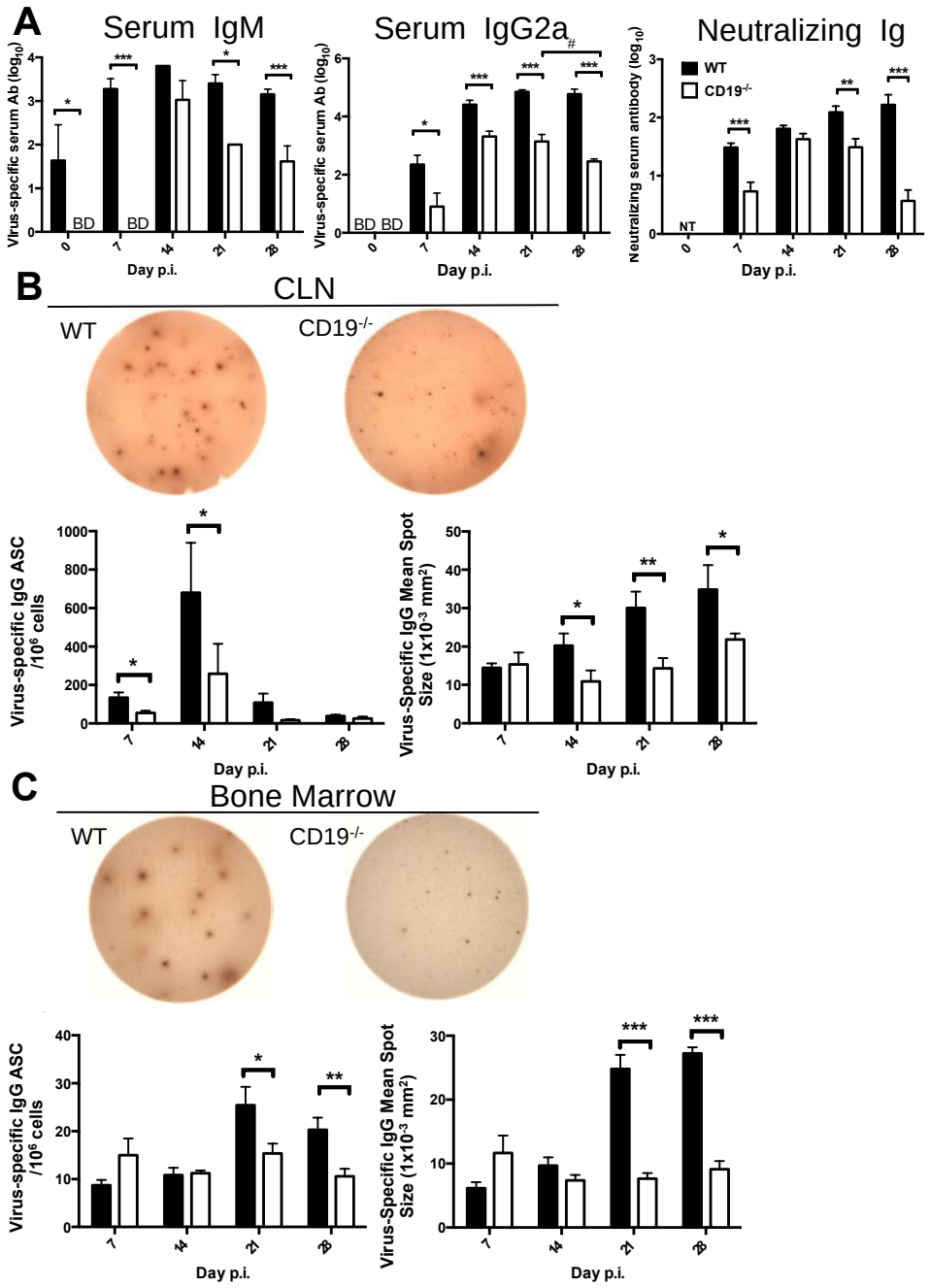

Figure 3. Reduced and unsustained virus-specific and neutralizing serum Ab coincides with decreased virus-specific ASC in the absence of CD19. A) Virus-specific IgM, IgG, and neutralizing Ab in sera of uninfected (Day 0 p.i.) and

infected mice at indicated times p.i. CLN (B) and bone marrow (C) were analyzed for virus specific IgG ASC by ELISPOT. Representative wells are shown for CLN at day 14 and bone marrow (BM) at day 21 p.i.. Graphs show frequencies of virus-specific IgG ASC spots and spot diameter. Data represent the mean $\pm$ SEM of individual mice from 3 separate experiments, each comprising 2-4 individual mice per time point and group. Statistically significant differences between WT and $CD19^{-/-}$ mice, determined by unpaired t test, are denoted by *$p < 0.05$, **$p < 0.01$, ***$p < 0.001$. Significant differences between time-points within the same group are denoted by # $p < 0.05$.

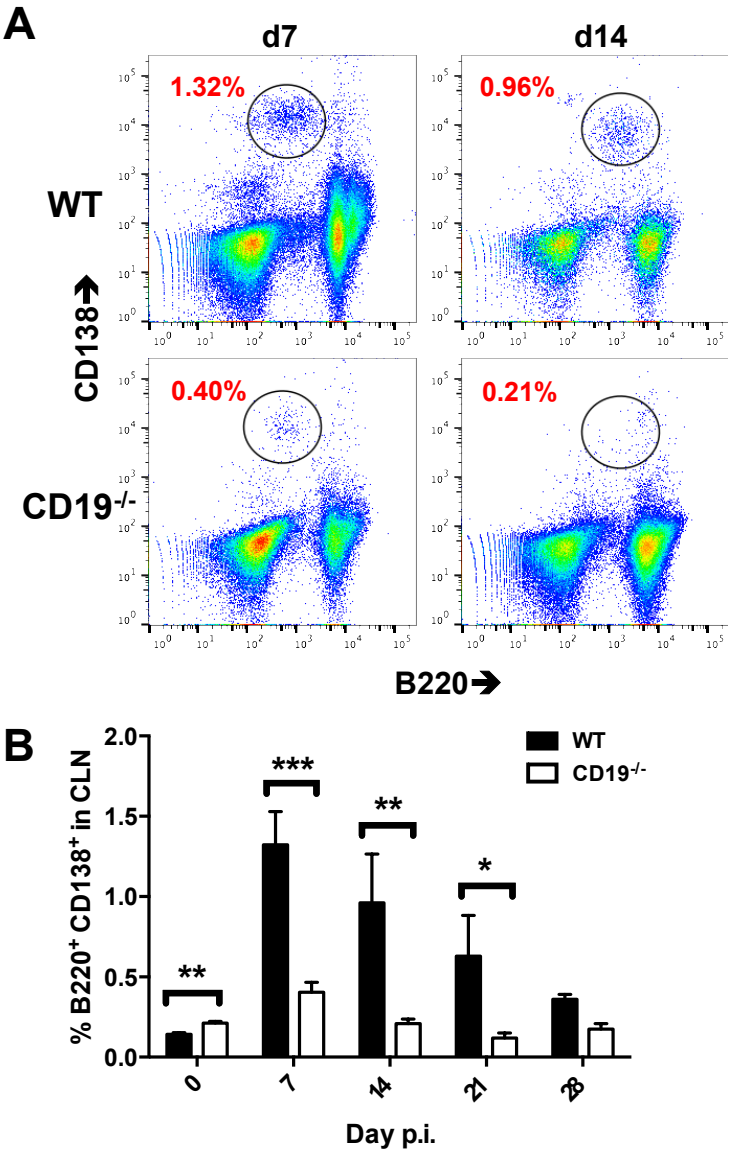

670

671 **Figure 4. CD138$^+$ ASCs are decreased in CLN of CD19$^{-/-}$ mice following**
672 **infection.** Pooled CLN cells from infected wt and CD19$^{-/-}$ mice (n=2-3 mice per
673 time point per group from 3 separate experiments) were stained for B220 and the
674 ASC marker CD138. A) Representative density plots depicting CD138$^+$ and
675 B220$^+$ B cells at 7 and 14 days p.i. (gated on live cells). Numbers represent
676 percentages of CD138$^+$ B220$^+$ ASCs within total cells. B) The bar graph shows
677 mean $\pm$ SEM. percentages of CD138$^+$ B220$^+$ ASCs within total CLN cells over

time. Statistically significant differences between wt and CD19$^{-/-}$ mice are denoted by *$p < 0.05$, *** $p < 0.001$.

682

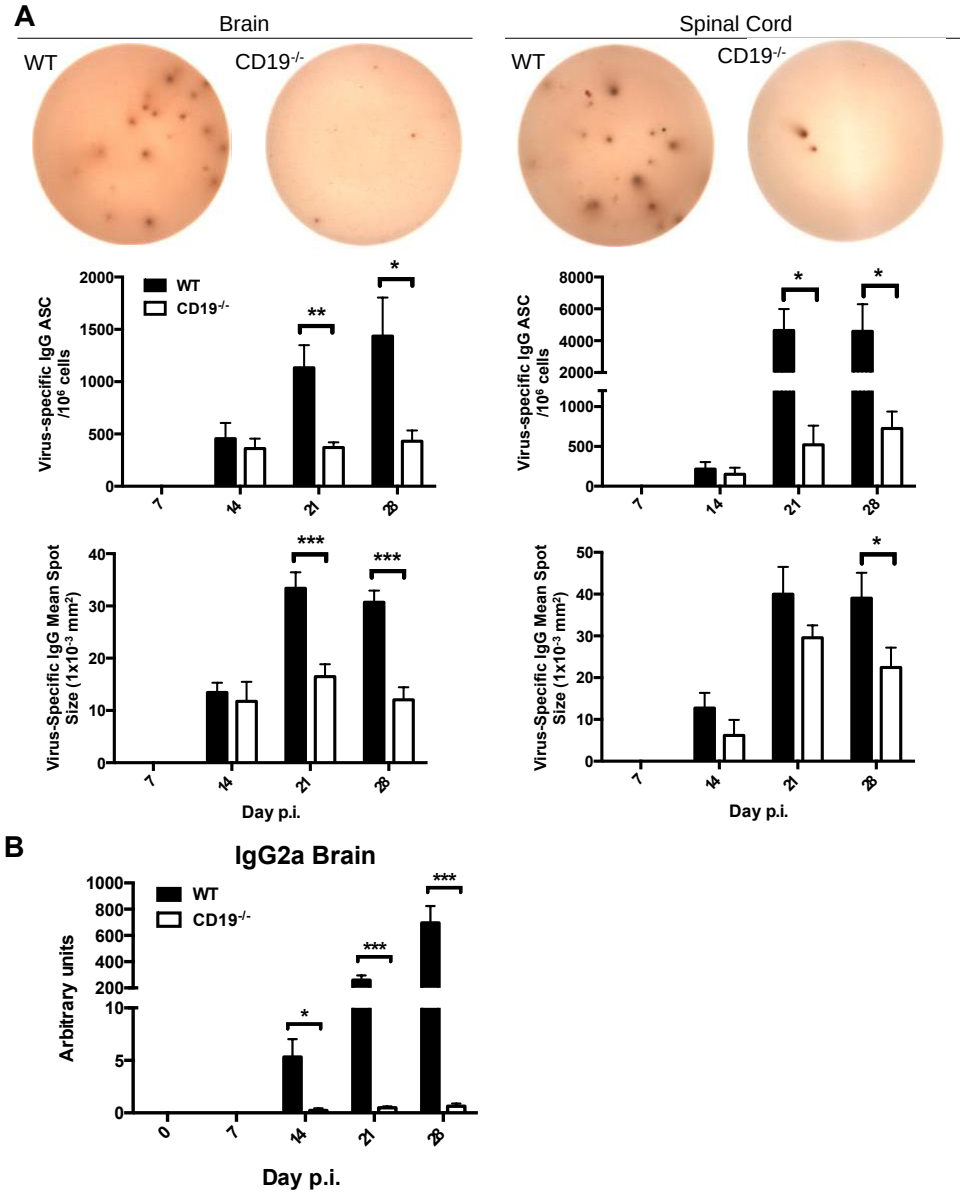

683

684 **Figure 5. Virus-specific ASC and Ab are severely decreased in the CNS of**
685 **CD19$^{-/-}$ mice.** A) Brain and spinal cord of infected wt and CD19$^{-/-}$ were analyzed
686 for virus-specific IgG ASC by ELISPOT. Representative wells are shown from
687 day 28 p.i.. Graphs show frequencies of virus-specific IgG ASC spots as well as
688 spot diameter. Statistically significant differences between WT and CD19$^{-/-}$ mice
689 (n=individual brains and pooled spinal cords from 2-6 mice per group per time

point from 4 separate experiments), determined by unpaired t test, are denoted by *p < 0.05, ** p < 0.01, *** p < 0.001. B) Virus-specific IgG2a in brain supernatants. Individual titers from 2-6 mice per group per time point from 2 separate experiments are shown. Statistically significant differences between WT and $CD19^{-/-}$ mice, determined by unpaired *t* test, are denoted by *p < 0.05, ** p < 0.01, *** p < 0.001.

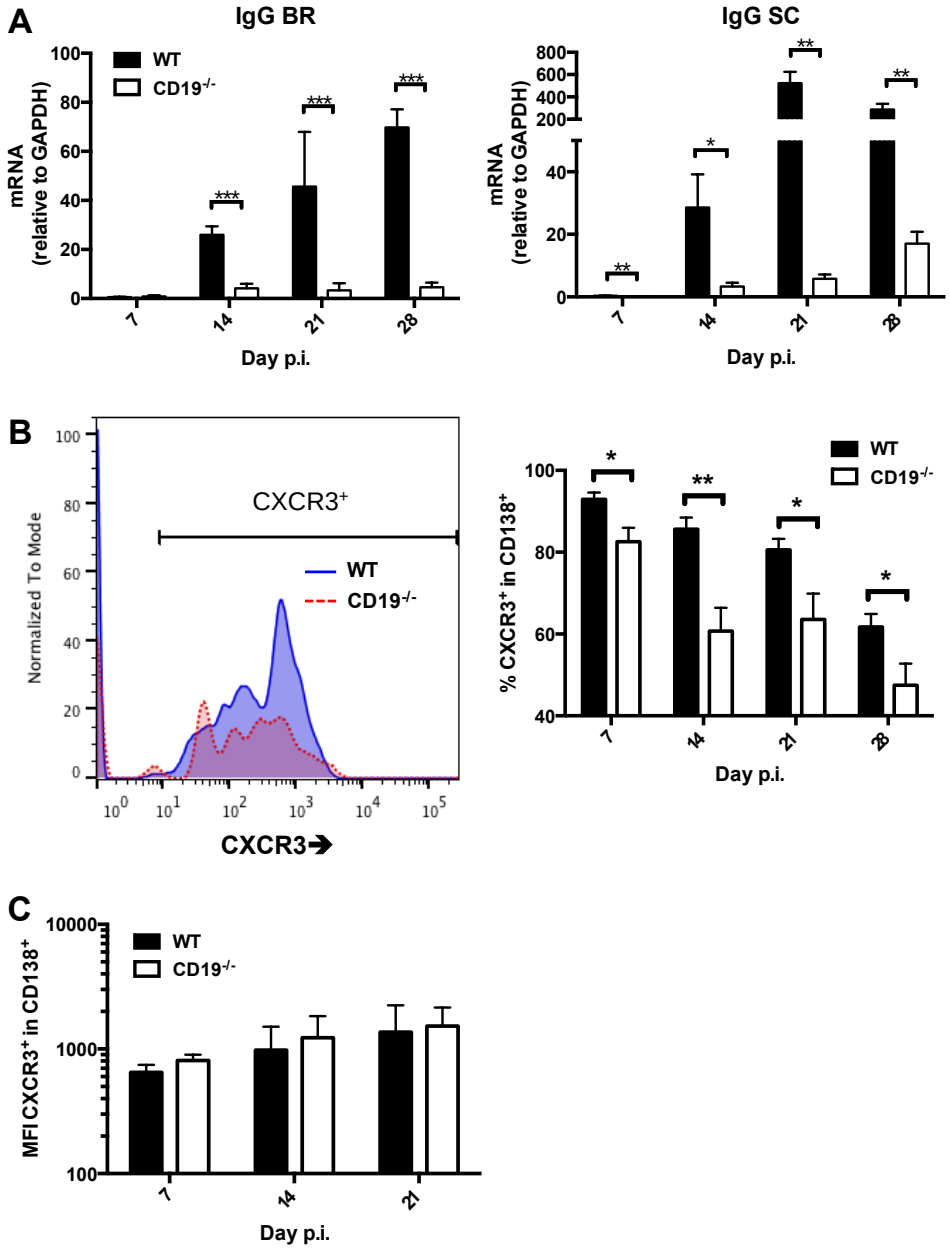

Figure 6. Total CXCR3$^+$ ASC are reduced in CLN of CD19$^{-/-}$ mice. A) Brains (BR) and spinal cords (SC) harvested from infected wt and CD19$^{-/-}$ mice at the indicated times p.i. were analyzed for expression of IgG heavy chain *(Ighg)* mRNA. Data represent the mean ± SEM transcript levels relative to *gapdh* mRNA of individual mice from 2 separate experiments, each comprising 2-6 individual

703 mice per time point and group. B) CLN cells pooled from infected mice were
704 stained for CD138 and CXCR3. Representative histograms gated on $B220^{+}$
705 $CD138^{+}$ ASCs at 21 days p.i. are shown for wt (blue, solid line) and $CD19^{-/-}$ mice
706 (red, dotted line); the graph depicts mean $\pm$ SEM percentages of $CXCR3^{+}$ cells
707 within ASC (n= 2-4 individual mice per group per time point from 3 separate
708 experiments). Statistically significant differences between WT and $CD19^{-/-}$ mice
709 are denoted by *$p < 0.05$, **$p < 0.01$. C) Mean fluorescent intensity (MFI) of
710 $CXCR3^{+}$ ASCs from cells depicted in B).
711

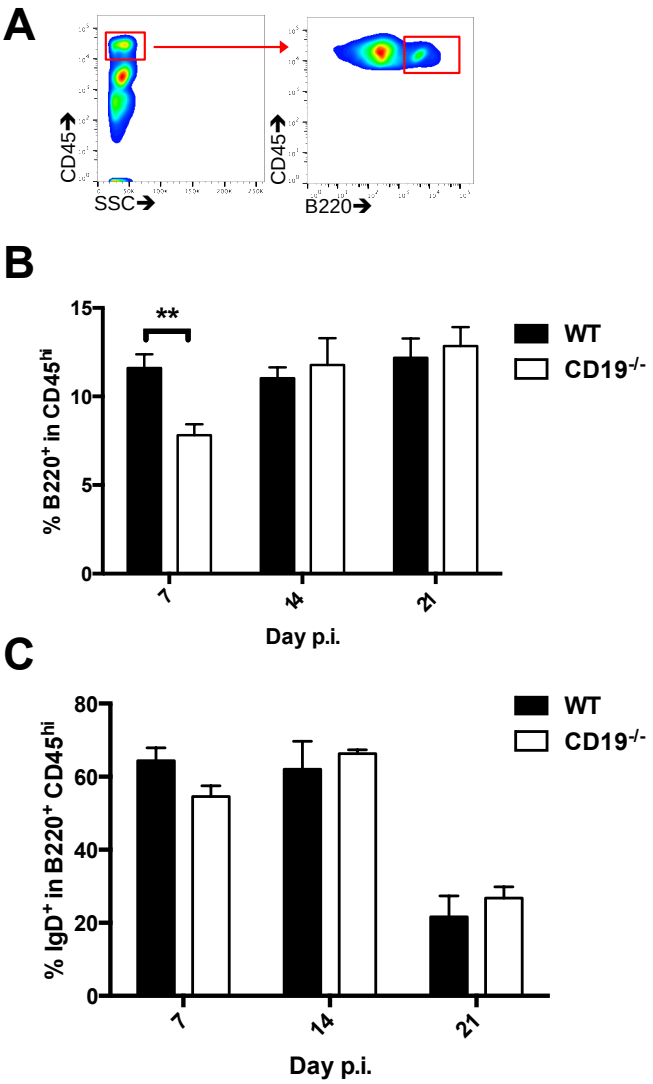

Figure 7. CD19 deficiency does not impair recruitment of IgD$^+$ B cells into the CNS. Brains from infected wt and CD19$^{-/-}$ mice were analyzed for accumulation of total CD45^{hi} expressing cells, as well as undifferentiated IgD$^+$ B220$^+$ B cells by flow cytometry. A) Representative density plots showing CD45 staining and side scatter (SSC) pattern and gating strategy for B220$^+$ cells within infiltrating CD45hi cells. Bar graphs depicts percentages of B220$^+$ cells within the CD45^{hi} infiltrating population (B) and percentages of IgD$^+$ cells within CD45^{hi} B220$^+$ B cells (C) over time. Data represent the mean $\pm$ SEM of individual mice from 2 separate experiments, each comprising 2-4 individual mice per time point and group. Statistically significant differences between wt and CD19$^{-/-}$ mice are denoted by **$p < 0.01$.

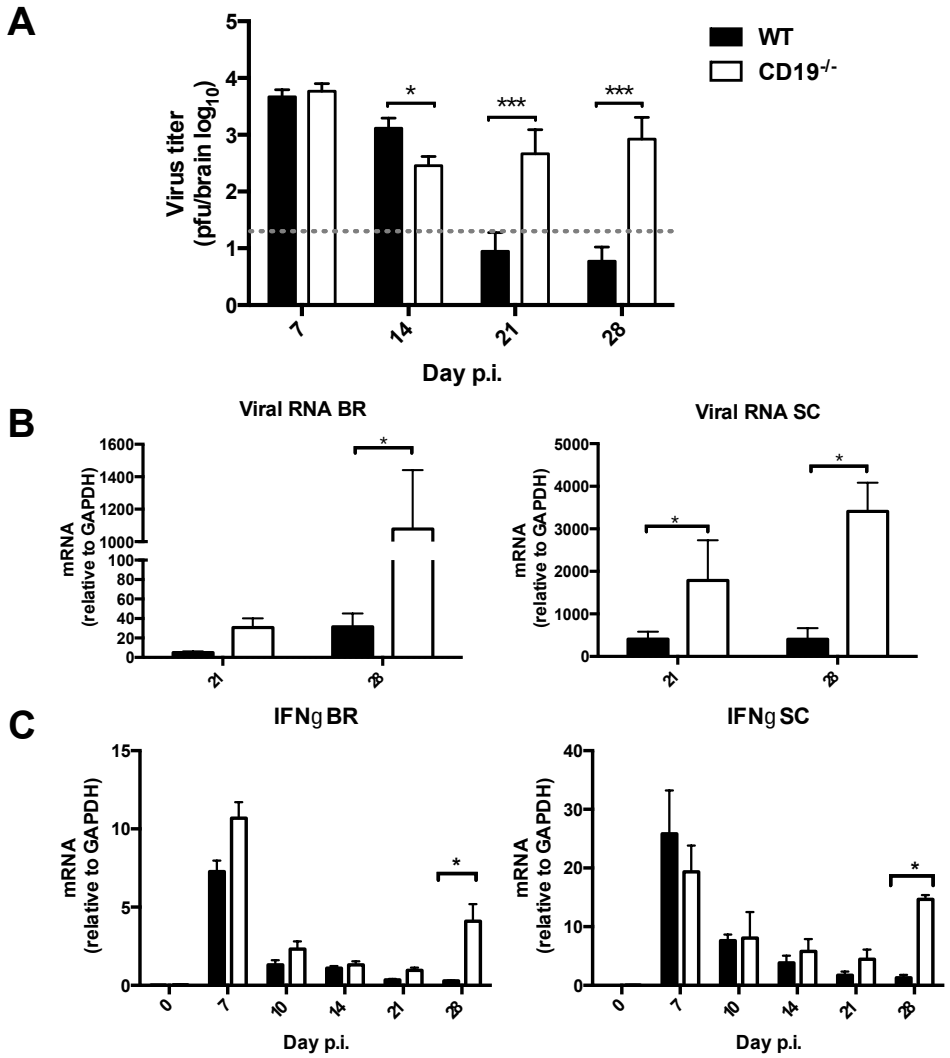

Figure 8. Impaired virus control associated with sparse local humoral immunity re-invigorates T-cell effector function. A) Infectious virus within the brains of WT and CD19$^{-/-}$ mice (n= 2-6 mice per group per time point from 4 separate experiments) determined by plaque assay. Dashed line indicates limit of detection. Levels of viral RNA encoding nucleocapsid protein (B) and IFNγ (C) in brains (BR) and spinal cords (SC) determined by real-time PCR. Data represent the mean ± SEM transcript levels relative to *gapdh* mRNA of individual mice from 2-3 separate experiments, each comprising 2-6 individual mice per time point and group. Statistically significant differences between wt and CD19$^{-/-}$ mice, determined by unpaired *t* test, are denoted by *p < 0.05, *** p < 0.001.

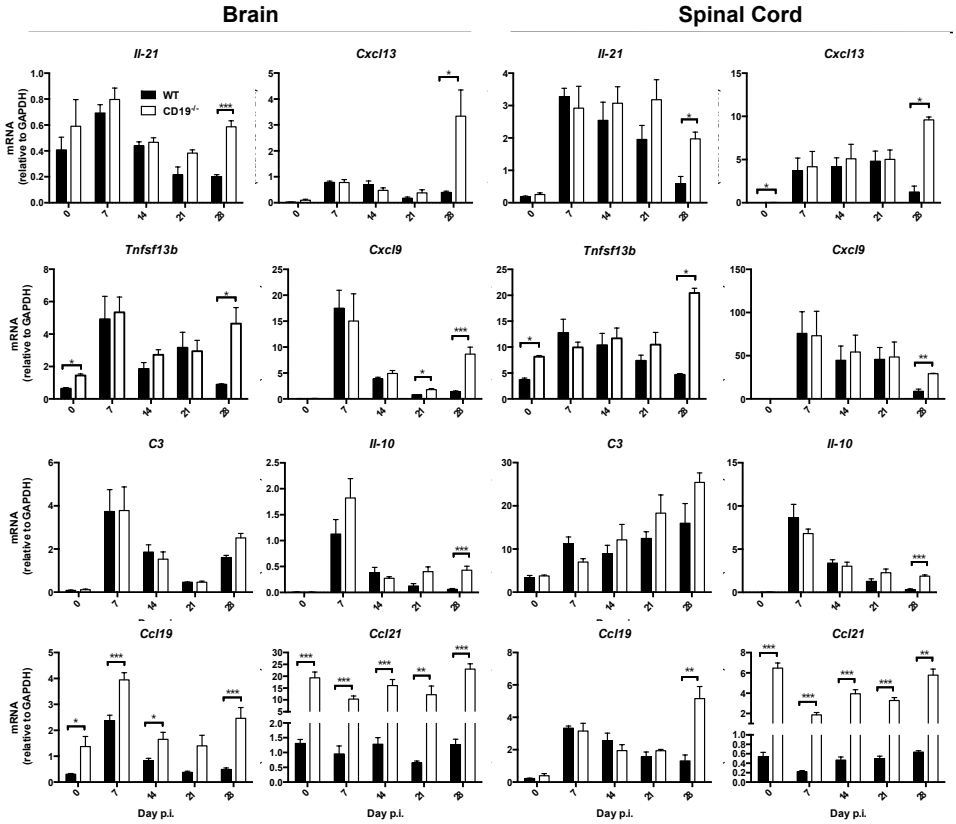

Figure 9. CD19 deficiency leads to re-emergence of T cell associated functions. Brains and spinal cords harvested from uninfected (Day 0 p.i.) and infected wt and CD19$^{-/-}$ mice at the indicated times p.i. were analyzed for mRNA encoding cytokines and chemokines associated with regulation of humoral responses. Data represent the mean ± SEM transcipt levels relative to *gapdh* mRNA of individual mice from 2-3 separate experiments, each comprising 2-6 individual mice per time point and group. Statistically significant differences between wt and CD19$^{-/-}$ mice, determined by unpaired *t* test, are denoted by *$p < 0.05$, **$p < 0.01$, *** $p < 0.001$.

1. Sedgwick JD, Dörries R. 1991. The immune system response to viral infection of the CNS. Seminars in Neuroscience 3:93-100.
2. Phares TW, Stohlman SA, Bergmann CC. 2013. Intrathecal humoral immunity to encephalitic RNA viruses. Viruses 5:732-752.
3. Griffin D, Levine B, Tyor W, Ubol S, Despres P. 1997. The role of antibody in recovery from alphavirus encephalitis. Immunol Rev 159:155-61.
4. Griffin DE. 2010. Recovery from viral encephalomyelitis: immune-mediated noncytolytic virus clearance from neurons. Immunol Res 47:123-133.
5. Bergmann CC, Lane TE, Stohlman SA. 2006. Coronavirus infection of the central nervous system: host–virus stand-off. Nat Rev Microbiol 4:121-132.
6. Marten NW, Stohlman SA, Zhou J, Bergmann CC. 2003. Kinetics of virus-specific CD8+-T-cell expansion and trafficking following central nervous system infection. J Virol 77:2775-2778.
7. Tschen S-I, Bergmann CC, Ramakrishna C, Morales S, Atkinson R, Stohlman SA. 2002. Recruitment kinetics and composition of antibody-secreting cells within the central nervous system following viral encephalomyelitis. J Immunol 168:2922-2929.
8. Phares TW, Marques CP, Stohlman SA, Hinton DR, Bergmann CC. 2011. Factors supporting intrathecal humoral responses following viral encephalomyelitis. J Virol 85:2589-98.
9. Okada T, Cyster JG. 2006. B cell migration and interactions in the early phase of antibody responses. Curr Opin Immunol 18:278-285.
10. Phares TW, DiSano KD, Hinton DR, Hwang M, Zajac AJ, Stohlman SA, Bergmann CC. 2013. IL-21 optimizes T cell and humoral responses in the central nervous system during viral encephalitis. J Neuroimmunol 263:43-54.
11. Marques CP, Kapil P, Hinton DR, Hindinger C, Nutt SL, Ransohoff RM, Phares TW, Stohlman SA, Bergmann CC. 2011. CXCR3-dependent plasma blast migration to the central nervous system during viral encephalomyelitis. J Virol 85:6136-47.
12. DiSano KD, Stohlman SA, Bergmann CC. 2017. Activated GL7+ B cells are maintained within the inflamed CNS in the absence of follicle formation during viral encephalomyelitis. Brain Behav Immun 60:71-83.
13. Phares TW, Stohlman SA, Hinton DR, Bergmann CC. 2013. Astrocyte-derived CXCL10 drives accumulation of antibody-secreting cells in the central nervous system during viral encephalomyelitis. J Virol 87:3382-3392.
14. Cyster JG. 2005. Chemokines, sphingosine-1-phosphate, and cell migration in secondary lymphoid organs. Annu Rev Immunol 23:127-159.
15. Victora GD, Nussenzweig MC. 2012. Germinal centers. Annu Rev Immunol 30:429-457.
16. Zotos D, Tarlinton DM. 2012. Determining germinal centre B cell fate. Trends Immunol 33:281-288.
17. Crotty S. 2012. The 1 - 1 - 1 fallacy. Immunol Rev 247:133-142.

18. Wengner AM, Höpken UE, Petrow PK, Hartmann S, Schurigt U, Bräuer R, Lipp M. 2007. CXCR5 - and CCR7 - dependent lymphoid neogenesis in a murine model of chronic antigen - induced arthritis. Arthritis Rheumatol 56:3271-3283.
19. Krumbholz M, Theil D, Cepok S, Hemmer B, Kivisäkk P, Ransohoff RM, Hofbauer M, Farina C, Derfuss T, Hartle C. 2005. Chemokines in multiple sclerosis: CXCL12 and CXCL13 up-regulation is differentially linked to CNS immune cell recruitment. Brain 129:200-211.
20. Haas J, Bekeredjian-Ding I, Milkova M, Balint B, Schwarz A, Korporal M, Jarius S, Fritz B, Lorenz H-M, Wildemann B. 2011. B cells undergo unique compartmentalized redistribution in multiple sclerosis. J Autoimmun 37:289-299.
21. Finch DK, Ettinger R, Karnell JL, Herbst R, Sleeman MA. 2013. Effects of CXCL13 inhibition on lymphoid follicles in models of autoimmune disease. Eur J Clin invest 43:501-509.
22. Kowarik MC, Cepok S, Sellner J, Grummel V, Weber MS, Korn T, Berthele A, Hemmer B. 2012. CXCL13 is the major determinant for B cell recruitment to the CSF during neuroinflammation. J Neuroinflammation 9:93.
23. Rupprecht TA, Plate A, Adam M, Wick M, Kastenbauer S, Schmidt C, Klein M, Pfister H-W, Koedel U. 2009. The chemokine CXCL13 is a key regulator of B cell recruitment to the cerebrospinal fluid in acute Lyme neuroborreliosis. J Neuroinflammation 6:42.
24. Phares TW, DiSano KD, Stohlman SA, Segal BM, Bergmann CC. 2016. CXCL13 promotes isotype-switched B cell accumulation to the central nervous system during viral encephalomyelitis. Brain Behav Immun 54:128-139.
25. Rainey-Barger EK, Rumble JM, Lalor SJ, Esen N, Segal BM, Irani DN. 2011. The lymphoid chemokine, CXCL13, is dispensable for the initial recruitment of B cells to the acutely inflamed central nervous system. Brain Behav Immun 25:922-931.
26. Fehr T, Rickert RC, Odermatt B, Roes J, Rajewsky K, Hengartner H, Zinkernagel RM. 1998. Antiviral protection and germinal center formation, but impaired B cell memory in the absence of CD19. J Exp Med 188:145-155.
27. Carter RH, Wang Y, Brooks S. 2002. Role of CD19 signal transduction in B cell biology. Immunol Res 26:45-54.
28. Rickert RC. 2005. Regulation of B lymphocyte activation by complement C3 and the B cell coreceptor complex. Curr Opin Immunol 17:237-243.
29. Del Nagro CJ, Otero DC, Anzelon AN, Omori SA, Kolla RV, Rickert RC. 2005. CD 19 function in central and peripheral B-cell development. Immunol Res 31:119-131.
30. Baiu DC, Prechl J, Tchorbanov A, Molina HD, Erdei A, Sulica A, Capel PJ, Hazenbos WL. 1999. Modulation of the humoral immune response by antibody-mediated antigen targeting to complement receptors and Fc receptors. J Immunol 162:3125-3130.

31. Ochsenbein AF, Pinschewer DD, Odermatt B, Carroll MC, Hengartner H, Zinkernagel RM. 1999. Protective T cell–independent antiviral antibody responses are dependent on complement. J Exp Med 190:1165-1174.
32. Fischer MB, Goerg S, Shen L, Prodeus AP, Goodnow CC, Kelsoe G, Carroll MC. 1998. Dependence of germinal center B cells on expression of CD21/CD35 for survival. Science 280:582-585.
33. Verschoor A, Brockman MA, Knipe DM, Carroll MC. 2001. Cutting edge: myeloid complement C3 enhances the humoral response to peripheral viral infection. J Immunol 167:2446-2451.
34. Rickert RC, Rajewsky K, Roes J. 1995. Impairment of T-cell-dependent B-cell responses and B-1 cell development in CD19-deficient mice. Nature 376:352.
35. Meinl E, Krumbholz M, Hohlfeld R. 2006. B lineage cells in the inflammatory central nervous system environment: migration, maintenance, local antibody production, and therapeutic modulation. Ann Neurol 59:880-892.
36. Rickert RC, Roes J, Rajewsky K. 1997. B lymphocyte-specific, Cre-mediated mutagenesis in mice. Nucleic Acids Res 25:1317-1318.
37. Fleming J, Trousdale M, El-Zaatari F, Stohlman S, Weiner L. 1986. Pathogenicity of antigenic variants of murine coronavirus JHM selected with monoclonal antibodies. J Virol 58:869-875.
38. Phares TW, Stohlman SA, Hinton DR, Atkinson R, Bergmann CC. 2010. Enhanced antiviral T cell function in the absence of B7-H1 is insufficient to prevent persistence but exacerbates axonal bystander damage during viral encephalomyelitis. J Immunol 185:5607-5618.
39. Bergmann CC, Altman JD, Hinton D, Stohlman SA. 1999. Inverted immunodominance and impaired cytolytic function of CD8+ T cells during viral persistence in the central nervous system. J Immunol 163:3379-3387.
40. Zhao J, Zhao J, Perlman S. 2014. Virus-specific regulatory T cells ameliorate encephalitis by repressing effector T cell functions from priming to effector stages. PLoS Pathog 10:e1004279.
41. Stern JN, Yaari G, Vander Heiden JA, Church G, Donahue WF, Hintzen RQ, Huttner AJ, Laman JD, Nagra RM, Nylander A. 2014. B cells populating the multiple sclerosis brain mature in the draining cervical lymph nodes. Sci Transl Med 6:248ra107-248ra107.
42. Louveau A, Smirnov I, Keyes TJ, Eccles JD, Rouhani SJ, Peske JD, Derecki NC, Castle D, Mandell JW, Kevin SL, Harris TH, Kipnis J. 2015. Structural and functional features of central nervous system lymphatics. Nature 523:337.
43. Engel P, Zhou L-J, Ord DC, Sato S, Koller B, Tedder TF. 1995. Abnormal B lymphocyte delevopment, activation, and differentiation in mice that lack or overexpress the CD19 signal transduction molecule. Immunity 3:39-50.
44. Berkowska MA, Driessen GJ, Bikos V, Grosserichter-Wagener C, Stamatopoulos K, Cerutti A, He B, Biermann K, Lange JF, van der Burg M, van Dongen JJM, van Zelm MC. 2011. Human memory B cells

originate from three distinct germinal center-dependent and-independent maturation pathways. Blood 118:2150-2158.

45. Ansel KM, Ngo VN, Hyman PL, Luther SA, Förster R, Sedgwick JD, Browning JL, Lipp M, Cyster JG. 2000. A chemokine-driven positive feedback loop organizes lymphoid follicles. Nature 406:309-314.

46. Tschen SI, Stohlman SA, Ramakrishna C, Hinton DR, Atkinson RD, Bergmann CC. 2006. CNS viral infection diverts homing of antibody - secreting cells from lymphoid organs to the CNS. Eur J Immunol 36:603-612.

47. Radbruch A, Muehlinghaus G, Luger EO, Inamine A, Smith KG, Dörner T, Hiepe F. 2006. Competence and competition: the challenge of becoming a long-lived plasma cell. Nat Rev Immunol 6:741-750.

48. Phares TW, DiSano KD, Stohlman SA, Bergmann CC. 2014. Progression from IgD+ IgM+ to isotype-switched B cells is site specific during coronavirus-induced encephalomyelitis. J Virol 88:8853-8867.

49. Smith AL, Barthold S, De Souza M, Bottomly K. 1991. The role of gamma interferon in infection of susceptible mice with murine coronavirus, MHV-JHM. Arch Virol 121:89-100.

50. Ramakrishna C, Bergmann CC, Atkinson R, Stohlman SA. 2003. Control of central nervous system viral persistence by neutralizing antibody. J Virol 77:4670-4678.

51. Muehlinghaus G, Cigliano L, Huehn S, Peddinghaus A, Leyendeckers H, Hauser AE, Hiepe F, Radbruch A, Arce S, Manz RA. 2005. Regulation of CXCR3 and CXCR4 expression during terminal differentiation of memory B cells into plasma cells. Blood 105:3965-3971.

52. Ramakrishna C, Stohlman SA, Atkinson RD, Shlomchik MJ, Bergmann CC. 2002. Mechanisms of central nervous system viral persistence: the critical role of antibody and B cells. J Immunol 168:1204-1211.

53. Lin MT, Hinton DR, Marten NW, Bergmann CC, Stohlman SA. 1999. Antibody prevents virus reactivation within the central nervous system. J Immunol 162:7358-7368.

54. Ramakrishna C, Bergmann CC, Atkinson R, Stohlman SA. 2003. Control of central nervous system viral persistence by neutralizing antibody. J Virol 77:4670-8.

55. Parra B, Hinton DR, Marten NW, Bergmann CC, Lin MT, Yang CS, Stohlman SA. 1999. IFN-γ is required for viral clearance from central nervous system oligodendroglia. J Immunol 162:1641-1647.

56. Bergmann CC, Parra B, Hinton DR, Chandran R, Morrison M, Stohlman SA. 2003. Perforin-mediated effector function within the central nervous system requires IFN-γ-mediated MHC up-regulation. J Immunol 170:3204-3213.

57. Puntambekar SS, Bergmann CC, Savarin C, Karp CL, Phares TW, Parra GI, Hinton DR, Stohlman SA. 2011. Shifting hierarchies of interleukin-10-producing T cell populations in the central nervous system during acute and persistent viral encephalomyelitis. J Virol 85:6702-6713.

58. Perlman S, Zhao J. 2017. Roles of regulatory T cells and IL-10 in virus-induced demyelination. J Neuroimmunol.
59. Puntambekar SS, Hinton DR, Yin X, Savarin C, Bergmann CC, Trapp BD, Stohlman SA. 2015. Interleukin - 10 is a critical regulator of white matter lesion containment following viral induced demyelination. Glia 63:2106-2120.
60. Lalor SJ, Segal BM. 2010. Lymphoid chemokines in the CNS. J Neuroimmunol 224:56-61.
61. Sköldenberg B, Kalimo K, Forsgren M, Halonen P. 1981. Herpes simplex encephalitis: A serological follow - up study. Acta Neurol Scand 63:273-285.
62. Schultze D, Weder B, Cassinotti P, Vitek L, Krausse K, Fierz W. 2004. Diagnostic significance of intrathecally produced herpes simplex and varizella-zoster virus-specific antibodies in central nervous system infections. Swiss Med Wkly 134:700.
63. Narayan K, Dail D, Li L, Cadavid D, Amrute S, Fitzgerald - Bocarsly P, Pachner AR. 2005. The nervous system as ectopic germinal center: CXCL13 and IgG in lyme neuroborreliosis. Ann Neurol 57:813-823.
64. Burke DS, Nisalak A, Lorsomrudee W, Ussery MA, Laorpongse T. 1985. Virus - specific antibody - producing cells in blood and cerebrospinal fluid in acute Japanese encephalitis. J Med Virol 17:283-292.
65. Vandvik B, Weil ML, Grandien M, Norrby E. 1978. Progressive rubella virus panencephalitis: Synthesis of oligoclonal virus - specific IgG antibodies and homogeneous free light chains in the central nervous system. Acta Neurol Scand 57:53-64.
66. Vandvik B, Norrby E. 1973. Oligoclonal IgG antibody response in the central nervous system to different measles virus antigens in subacute sclerosing panencephalitis. Proc Natl Acad Sci U S A 70:1060-1063.
67. Thakare JP, Gore MM, Risbud AR, Banerjee K, Ghosh SN. 1991. Detection of virus specific IgG subclasses in Japanese encephalitis patients. Indian J Med Res 93:271-6.
68. Kaiser R, Dorries R, Luer W, Poser S, Pohle HD, Felgenhauer K, ter Meulen V. 1989. Analysis of oligoclonal antibody bands against individual HIV structural proteins in the CSF of patients infected with HIV. J Neurol 236:157-60.
69. Ryzhova E, Aye P, Harvey T, Cao W, Lackner A, Gonzalez-Scarano F. 2009. Intrathecal humoral responses are inversely associated with the frequency of simian immunodeficiency virus macrophage-tropic variants in the central nervous system. J Virol 83:8282-8.
70. Puccioni-Sohler M, Rios M, Bianco C, Zhu SW, Oliveira C, Novis SA, Pombo-de-Oliveira MS. 1999. An inverse correlation of HTLV-I viral load in CSF and intrathecal synthesis of HTLV-I antibodies in TSP/HAM. Neurology 53:1335-9.
71. Hooper DC, Phares TW, Fabis MJ, Roy A. 2009. The production of antibody by invading B cells is required for the clearance of rabies virus from the central nervous system. PLoS Negl Trop Dis 3:e535.

72. Fragkoudis R, Ballany CM, Boyd A, Fazakerley JK. 2008. In Semliki Forest virus encephalitis, antibody rapidly clears infectious virus and is required to eliminate viral material from the brain, but is not required to generate lesions of demyelination. J Gen Virol 89:2565-8.
73. Levine B, Hardwick JM, Trapp BD, Crawford TO, Bollinger RC, Griffin DE. 1991. Antibody-mediated clearance of alphavirus infection from neurons. Science 254:856-60.
74. Pachner AR, Brady J, Narayan K. 2007. Antibody-secreting cells in the central nervous system in an animal model of MS: Phenotype, association with disability, and in vitro production of antibody. J Neuroimmunol 190:112-20.
75. Lee H, Sunden Y, Ochiai K, Umemura T. 2011. Experimental intracerebral vaccination protects mouse from a neurotropic virus by attracting antibody secreting cells to the CNS. Immunol Lett 139:102-9.
76. Corcione A, Casazza S, Ferretti E, Giunti D, Zappia E, Pistorio A, Gambini C, Mancardi GL, Uccelli A, Pistoia V. 2004. Recapitulation of B cell differentiation in the central nervous system of patients with multiple sclerosis. Proc Natl Acad Sci U S A 101:11064-9.
77. Owens GP, Bennett JL, Gilden DH, Burgoon MP. 2006. The B cell response in multiple sclerosis. Neurol Res 28:236-44.
78. Owens GP, Ritchie AM, Burgoon MP, Williamson RA, Corboy JR, Gilden DH. 2003. Single-cell repertoire analysis demonstrates that clonal expansion is a prominent feature of the B cell response in multiple sclerosis cerebrospinal fluid. J Immunol 171:2725-33.
79. Krumbholz M, Theil D, Derfuss T, Rosenwald A, Schrader F, Monoranu CM, Kalled SL, Hess DM, Serafini B, Aloisi F, Wekerle H, Hohlfeld R, Meinl E. 2005. BAFF is produced by astrocytes and up-regulated in multiple sclerosis lesions and primary central nervous system lymphoma. J Exp Med 201:195-200.
80. Thangarajh M, Masterman T, Hillert J, Moerk S, Jonsson R. 2007. A proliferation-inducing ligand (APRIL) is expressed by astrocytes and is increased in multiple sclerosis. Scand J Immunol 65:92-8.
81. Metcalf TU, Baxter VK, Nilaratanakul V, Griffin DE. 2013. Recruitment and retention of B cells in the central nervous system in response to alphavirus encephalomyelitis. J Virol 87:2420-2429.
82. Cervantes-Barragán L, Kalinke U, Züst R, König M, Reizis B, López-Macías C, Thiel V, Ludewig B. 2009. Type I IFN-mediated protection of macrophages and dendritic cells secures control of murine coronavirus infection. J Immunol 182:1099-1106.
83. Coro ES, Chang WW, Baumgarth N. 2006. Type I IFN receptor signals directly stimulate local B cells early following influenza virus infection. J Immunol 176:4343-4351.
84. Purtha WE, Chachu KA, Virgin HW, Diamond MS. 2008. Early B-cell activation after West Nile virus infection requires alpha/beta interferon but not antigen receptor signaling. J Virol 82:10964-10974.

85. Veerhuis R, Janssen I, De Groot CJ, Van Muiswinkel FL, Hack CE, Eikelenboom P. 1999. Cytokines associated with amyloid plaques in Alzheimer's disease brain stimulate human glial and neuronal cell cultures to secrete early complement proteins, but not C1-inhibitor. Exp Neurol 160:289-299.
86. Hosokawa M, Klegeris A, Maguire J, McGeer PL. 2003. Expression of complement messenger RNAs and proteins by human oligodendroglial cells. Glia 42:417-423.
87. Veerhuis R, Nielsen HM, Tenner AJ. 2011. Complement in the brain. Mol Immunol 48:1592-1603.
88. DiSano KD, Stohlman SA, Bergmann CC. 2017. An optimized method for enumerating CNS derived memory B cells during viral-induced inflammation. J Neurosci Methods 285:58-68.
89. Baccala R, Hoebe K, Kono DH, Beutler B, Theofilopoulos AN. 2007. TLR-dependent and TLR-independent pathways of type I interferon induction in systemic autoimmunity. Nat Med 13:543.
90. Das A, Heesters BA, Bialas A, O'Flynn J, Rifkin IR, Ochando J, Mittereder N, Carlesso G, Herbst R, Carroll MC. 2017. Follicular dendritic cell activation by TLR ligands promotes autoreactive B cell responses. Immunity 46:106-119.
91. Cupovic J, Onder L, Gil-Cruz C, Weiler E, Caviezel-Firner S, Perez-Shibayama C, Rülicke T, Bechmann I, Ludewig B. 2016. Central nervous system stromal cells control local CD8+ T cell responses during virus-induced neuroinflammation. Immunity 44:622-633.
92. Wingerchuk DM, Carter JL. 2014. Multiple sclerosis: current and emerging disease-modifying therapies and treatment strategies. Mayo Clin Proc 89:225-240
93. Chalkias S, Dang X, Bord E, Stein MC, Kinkel RP, Sloane JA, Donnelly M, Ionete C, Houtchens MK, Buckle GJ. 2014. JC virus reactivation during prolonged natalizumab monotherapy for multiple sclerosis. Annals of neurology 75:925-934.